

# COMBUSTION MODELING IN LARGE SCALE VOLUMES

A. Velikorodny<sup>1</sup>, E.Studer<sup>2</sup>, S.Kudriakov<sup>2</sup>, A.Beccantini<sup>2</sup>

<sup>1</sup>AUSY, 88 bd. Gallieni, F-92445 Issy Les Moulineaux,  
France, e-mail : alexey.velikorodny@cea.fr, <sup>2</sup>CEA,  
DEN, DM2S/STMF, F-91191 Gif-Sur-Yvette,  
Cedex, France, e-mail : etienne.studer@cea.fr

## ABSTRACT

This paper is devoted to a benchmarking exercise of the EUROPLEXUS code against several large scale deflagration and detonation experimental data sets in order to improve its hydrogen combustion modeling capabilities in industrial settings. The code employs an algorithm for the propagation of reactive interfaces, RDEM, which includes a combustion wave, as an integrable part of the Reactive Riemann problem, propagating with a fundamental flame speed (being a function of initial mixture properties as well as gas dynamics parameters). An improvement of the combustion model is searched in a direction of transient interaction of flames with regions of elevated vorticity/shear in obstacle-laden channels and vented enclosures.

## 1.0 INTRODUCTION

During certain accidental scenarios in a nuclear reactor containment, hydrogen gas is released into the reactor building. In the case of ignition various combustion regimes are possible depending on the local concentrations of hydrogen and steam, as well as temperature and pressure distributions. These regimes may include jet fires, slow or fast deflagrations and detonations. Therefore, in order to improve the hydrogen risk management strategies one has to find means to estimate the severity of combustion processes involved under given initial conditions.

The use of CFD methods for industrial applications implies a capability to deal with geometries very large with respect to characteristic dimensions involved in flame acceleration processes. Although, many types of approximations might be employed (e.g. for thermal and species diffusion, viscosity, turbulence, etc.), the pressure loads could be correctly predicted in general should the flame speed be properly resolved. A large scale approach to combustion modeling was first proposed in [12] and resulted in the CREBCOM model. This algorithm is simple to implement as it resolves non-reactive Euler equations with a reactive contribution added by introducing a source term. This model was successfully employed in several industrial CFD codes, including TONUS, [17] and COM3D, [5].

Recently, numerical benchmarks which have been performed, in particular, within a framework of OECD/NEA (ISP49(2012), [15]), demonstrated that current numerical models experience poor predictive capabilities at the industrial scale, both due to under-resolution

and deficiencies in combustion modeling. This paper describes a benchmarking exercise of a new model, which was recently implemented in the EUROPLEXUS code [13]. Its validation is based on the experimental data obtained in several large scale facilities, which are listed hereafter.

## 2.0 NUMERICAL MODELING

### 2.1 RDEM model

A combustion model was developed in CEA and described in [4] to deal with hydrogen hazards in large scale facilities. The equations to be solved are the reactive Euler equations:

$$\begin{cases} \frac{\partial}{\partial t} \rho + \vec{\nabla} \cdot (\rho \vec{w}) = 0 \\ \frac{\partial}{\partial t} (\rho \vec{w}) + \vec{\nabla} \cdot (\rho \vec{w} \otimes \vec{w} + P) = 0 \\ \frac{\partial}{\partial t} (\rho \tilde{e}_t) + \vec{\nabla} \cdot (\rho \vec{w} \tilde{h}_t) = 0 \\ \frac{\partial}{\partial t} (\xi) + \vec{D} \cdot \vec{\nabla} \xi = 0 \end{cases} \quad (1)$$

The first three equations are the classical conservation equations for mass, momentum and energy. The fourth equation is the transport equation for the progress variable  $\xi$ . This equation is in non-conservative form. The apparent flame speed  $\vec{D}$  has to be defined only on the interface (with the same value ahead and behind it) and represents its velocity. In this work we compute  $\vec{D}$  as a function of the fundamental flame speed  $K_0$  via

$$\vec{D} = \vec{w} + K_0 \vec{n} \quad (2)$$

where  $\vec{n}$  is a normal to the flame surface going from a burnt to an unburnt region,  $\vec{w}$  is the velocity of the unburnt gas. It is assumed that we know the fundamental flame speed  $K_0$  as a function of space and time.

In literature there exist several approaches to model a flame as an interface. Some of these approaches reacquire a solution of the reactive Riemann problem between a burnt and an unburnt region. We use the reactive discrete equation method (RDEM) [18] to propagate the flame front. This method is conservative, since in a close and isolated system the total mass and energy are conserved. It does not suffer from the problem of pressure and velocity oscillations at the combustion interface when the specific heat ratios are different. Finally, an implementation of the RDEM in an existing Finite Volume code is rather straightforward and does not require an interface reconstruction.

### 2.2 Fundamental Flame Velocity Modeling

The only parameter of the RDEM model is  $K_0$  which represents a fundamental flame velocity, i.e. the flame velocity relative to the fresh mixture just ahead of it. In this subsection we describe a model for this parameter being expressed as a product of several factors, [3]:

$$K_0 = S_L^0 \Theta_{TH} \Theta_{TURB} \Theta_{WRIN} \quad (3)$$

where  $S_L^0$  is the laminar flame speed of a gas mixture under consideration determined at reference temperature and pressure  $(P_0, T_0)$ ,  $\Theta_{TH}$  is the thermodynamic factor which takes into account an influence of elevated pressure and temperature,  $\Theta_{TURB}$  is the turbulence factor, and  $\Theta_{WRIN}$  is the flame wrinkling factor.

A typical form of the model, which takes into account an influence of elevated temperature and pressure on the laminar flame speed determined according to their reference values  $(T_0, P_0)$  is

$$\Theta_{TH} = \left(\frac{P}{P_0}\right)^\alpha \left(\frac{T}{T_0}\right)^\beta \quad (4)$$

For mixtures containing hydrogen gas experimental results give  $\alpha = -0.5$  and  $\beta = 2.2$  [20].

The wrinkling factor in the present study accounts for a flame surface area increase in the fully-turbulent velocity region. In the case of flame propagation in an unbounded free space, it has been shown by Gostintsev and co-authors [14] that the ratio between the surface of a spherically propagating flame and the surface of the equivalent sphere increases according to  $(R/R_0)^{1/3}$ , where  $R$  is a distance from the ignition point, and  $R_0$  is a distance at which the fully-turbulent regime is reached.  $R_0$  has been shown to be of the order of 1 m for a stoichiometric hydrogen-air mixture, [14]. However, at present there exist no model or an experimental correlation for this parameter for various mixtures and/or in the presence of acoustic waves. In this work a constant value of  $R_0 = 1$  m was chosen. Finally,

$$\Theta_{WRIN} = \left(\frac{R}{R_0}\right)^{1/3} \quad (5)$$

where  $R$  is a distance between an ignition point and a flame front.

The turbulence factor is described next. In the present study we prefer to use an algebraic model in the form of correlation for turbulent flame velocity, as given in [6]:

$$\Theta_{TURB} = 1 + 1.334\gamma \left(\frac{u'}{S_L^0}\right)^{0.55} \left(\frac{L_t}{\delta_L}\right)^{0.15} (\text{Le})^{-0.3} \quad (6)$$

where  $u'$  is the r.m.s. (root mean square) turbulent velocity,  $L_t$  is the integral scale of turbulence,  $\delta_L$  is the thickness of laminar flame, and  $\text{Le}$  is the Lewis number. A coefficient  $\gamma$  is introduced in order to take into account the notion of effective r.m.s. turbulent velocity due to the fact that influence of different turbulent scales depends on the flame size. In [1] different values are proposed for this parameter depending on experimental conditions. In the present study we keep the value of  $\gamma = 0.6$ . For the Lewis number we consider the approach given in [2], where an expression for the effective Lewis number is proposed:

$$\text{Le}_{eff} = 1 + \frac{(\text{Le}_E - 1) + (\text{Le}_D - 1)\mathcal{A}}{1 + \mathcal{A}} \quad (7)$$

This equation covers the domain of all concentrations with the subscript  $D$  standing for deficient reactant, and the subscript  $E$  corresponding to the reactant, which is in a relative excess. Here  $\mathcal{A} = 1 + \beta(\Phi - 1)$  is a measure of the mixture strength, and  $\Phi$  is defined as

the ratio of the mass of excess-to-deficient reactants in the fresh mixture relative to their stoichiometric ratio. The Zeldovich number  $\beta$  is computed based on the results from [10].

The r.m.s. turbulent velocity is found from, [21]:

$$u' = L_t \|S_{ij}\|, \quad \text{with} \quad S_{ij} = \frac{1}{2} \left[ \frac{\partial u_i}{\partial x_j} + \frac{\partial u_j}{\partial x_i} \right]. \quad (8)$$

In order to estimate the integral scale of turbulence,  $L_t$ , two methods are adopted. In the first approximation it is set to be proportional a mesh size size  $\Delta$ ; i.e.  $L_t = C_u \times \Delta$ , where a constant  $C_u$  was determined based on the numerical modeling experiments. It is found, in particular, that in geometries with obstacles  $C_u$  is of the order of unity, should the mesh size was correctly chosen, while in the obstacle-free ones it must be reduced by one order of magnitude. The second approach to the integral scale modeling was based on the shear layer theory. Brown and Roshko [7] demonstrated, that the turbulent mixing layer is formed of quasi-deterministic vortices or coherent structures. It has been shown, in particular, that it is possible to characterize growth/development of the separated shear layers, related to the transformation from the small-scale vortices to the large-scale clusters of vorticity, in terms of variation of vorticity thickness as a function of the downstream distance,  $\delta(x)$ . The latter is defined as follows:

$$\delta(x) = \frac{U_1 - U_2}{\max\left(\frac{dU}{dy}\right)}, \quad (9)$$

where  $U_1$  and  $U_2$  are the equivalents of the free-stream velocity on the upper and the lower sides of the mixing layer and  $\frac{dU}{dy}$  is the mean velocity gradient in the transverse direction.

Finally, in the second approach the turbulent integral scale was dynamically updated in the regions of the elevated vorticity and shear using a local value of  $\delta(x)$ , while the previous method with a constant  $L_t$  was employed elsewhere in the computational domain.

It should be noted, that this paper shows the results obtained with a vorticity thickness model given by equation (9), which is two-dimensional in its nature. Another "3D" model is in the process of being generalized for scenarios where a flame trajectory and a direction of the maximum velocity gradient are not known a priori. In this case a contribution of the wrinkling factor is accounted for in the  $\Theta_{TURB}$  term, and, thus,  $\Theta_{WRIN}$  will be set to unity in future.

### 3.0 EXPERIMENTS

#### 3.1 RUT facility

The Russian RUT facility [11] represents a reinforced concrete building having a few channels and compartments inside (see Figure 1). The geometry consists of the first channel (34.6 m long and 5.6 m<sup>2</sup> in cross section), the canyon (10.55 m long and 15.7 m<sup>2</sup> cross section) and a second channel with a linear part being 18 m long. Concrete obstacles were located in the first channel in order to promote the flame acceleration processes. The blockage ratio (BR) was usually equal to 0.3, while a few tests were performed using  $BR = 0.6$ . The ignition was

initiated with a weak electrical spark at the closed end of a first channel. The mixture of hydrogen/air and steam was homogeneous in all experiments considered herein. The facility was equipped with pressure transducers to record the pressure waves development during the combustion process. The flame front position was deduced from photodiodes and ion probes, [11].

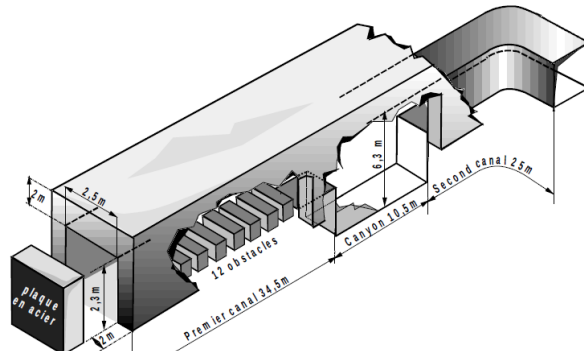


FIG. 1: Geometry of RUT facility

Various experimental programs were performed between 1993 and 2003. 17 tests have been selected for the present validation purposes, but only 7 are described in this article (see Table I) involving the following regimes: slow flame, fast flame and transition from deflagration to detonation (TDD).

TABLE I: Initial conditions and main results of RUT tests

Test	$[H_2]_{dry}$ (vol%)	$[H_2O]$ (vol%)	$T$ (K)	Comment
T13	11	0	283	Fast flame
T22	14	0	283	DDT
T23	11.2	0	283	Fast flame
STM7	17.5	25.7	362	Fast flame
STM3	16.9	15.1	356	Critical zone
STM2	14.7	14.8	363	Fast flame
STH9	10.1	6.7	364	Slow flame

During the STM7 test (typical fast flame regime), the flame was continuously accelerated and the “choked-flame” conditions were reached in the middle of the first channel (see Figures 2). This regime was maintained during the flame propagation in the canyon and in the second channel. The maximum pressure was about 9 bar when the flame reached the choking regime. The STH9 test had a low hydrogen and a water vapor contents (with concentrations being representative of the TMI accident), which resulted in a typical slow flame regime in the RUT facility. Deflagration with a flame speed of the order of 270 m/s and suppression of 1 bar were observed (see Figure 3).

In addition to the RUT facility the code was validated based on the experimental data from the DRIVER [19], ENACCEF [15], BATELLE [15], THAI [15], HDR [9] and FMGlobal [3] test cases. We have chosen the results from the last two exercises, as being representative for the large scale verification of the combustion model in the relatively slow flame regimes.

### 3.2 HDR and FMGlobal facilities

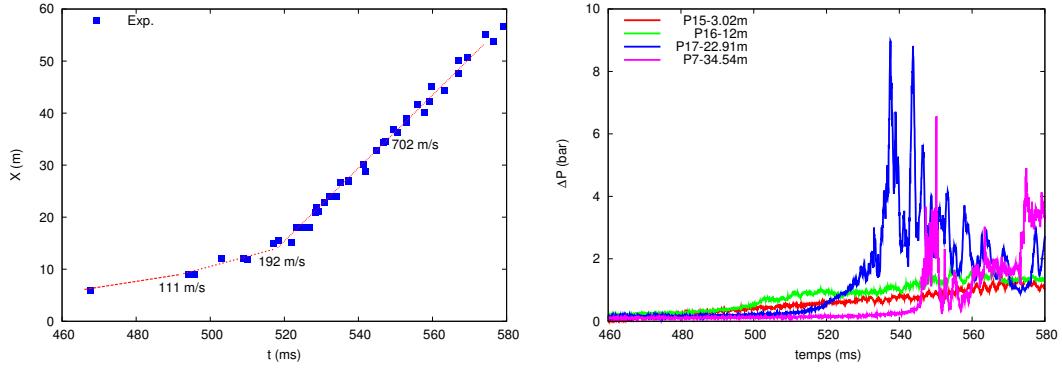


FIG. 2: STM7 test: Flame front location and overpressures

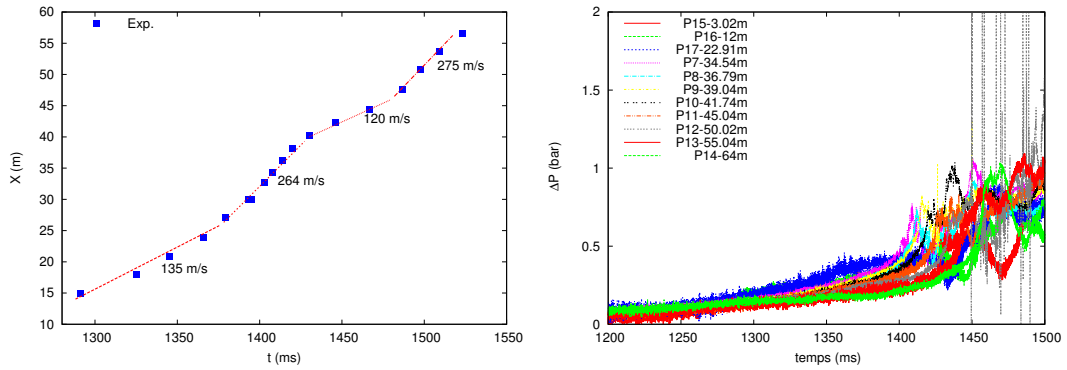


FIG. 3: STH9 test: Flame front location and overpressures

The E12-3.2 hydrogen experiment was performed in the Heiss Dampf Reactor (HDR), [9]. Its geometry consists of the chain of interconnected compartments R1-904, R1-905 and R1-801 (see Figure 4). The dimensions of the rooms are given in Table II. The cross-section

TABLE II: HDR geometry: Sizes of chamebers

Room	Length (m)	Width (m)	Height (m)	Volume (m <sup>3</sup> )
R1-904	5.5	5.5	4.65	140
R1-905	4.1	4.0	4.55	75
R1-801	7.0	5.5	9.50	330

areas of the vents are: 2.34 m<sup>2</sup> for transition from R1-905 to R1-801, and 4.68 m<sup>2</sup> for the one from R1-801 to the dome. The initial gas mixture is 10 vol% of hydrogen, 25 vol% of steam and 65 vol% of air at the pressure of 1 bar and the temperature of 337 K. The main experimental results provided by this test series was the large overpressure due to the jet combustion between R1-905 and R1-801 compartments, when the flame was ignited at the far-end of the R1-904 chamber. Other ignition locations (at the door between R1-905 and R1-801 or in R1-801) have shown lower overpressure.

The data in the FMGlobal experiment was obtained in the 64 m<sup>3</sup> test chamber. Its overall dimensions were 4.6x3.0x4.6 m with a square vent of either 5.4 m<sup>2</sup>, or 2.7 m<sup>2</sup> located on the vertical wall of a chamber. Four pressure transducers and twenty flame of arrival thermocouples were installed at various locations inside the chamber (see Figure 5). The initial gas

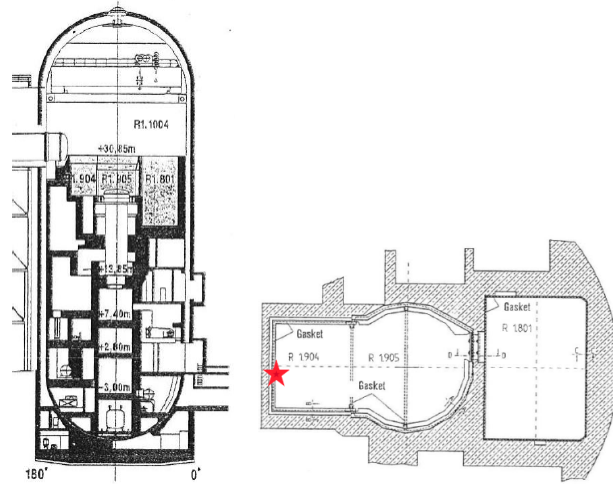


FIG. 4: Geometry of HDR facility

mixture composition was 18 vol% of hydrogen-air at the ambient pressure and temperature. Experiments were performed for the two vent sizes and the three ignition locations: back, center and front.

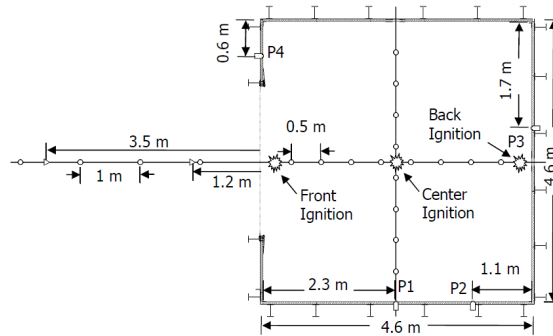


FIG. 5: Geometry of FMGlobal test chamber

## 4.0 RESULTS AND DISCUSSIONS

This section presents a discussion of the computations which were performed and their comparison with experimental data. All results have been obtained on a 3D uniform grid with the numerical model implemented in CAST3M [8] and EUROPLEXUS [13] codes. The time scales in the computation have been adjusted in order to correct for initial flame development phase, i.e. transition from laminar to turbulent flame.

### 4.1 RUT facility

The data which was used in the model for these tests is given in Table III, where  $\sigma$  is an expansion ratio and  $\beta$  is a Zeldovich number. The only model constant  $C_u$  was set to 1.0 for all tests presented in this subsection. However, it should be noted, that it may change in the range from 0.2 to 1.4 for the constant integral scale model in the scenarios not shown

herein.

TABLE III: Global combustion parameters of RUT tests

Test	$S_L^0$ (m/s)	$\delta_L$ (mm)	$\sigma$	$Le_{eff}$	$\beta$
T13	0.178	0.17	3.86	0.456	4.98
T22	0.302	0.11	4.54	0.523	4.37
T23	0.185	0.16	3.9	0.46	4.93
STM7	0.308	0.13	3.41	0.467	4.15
STM3	0.408	0.1	3.72	0.5	3.97
STM2	0.301	0.14	3.39	0.451	4.19
STH9	0.162	0.25	2.88	0.392	4.65

First we have addressed the effect of the grid size. Calculations of the STM7 and STH9 tests have been performed with uniform grids of  $\Delta x = 40, 20$  and  $10$  cm, utilizing in the first approximation a model with a constant integral length scale ( $L_t$ ).

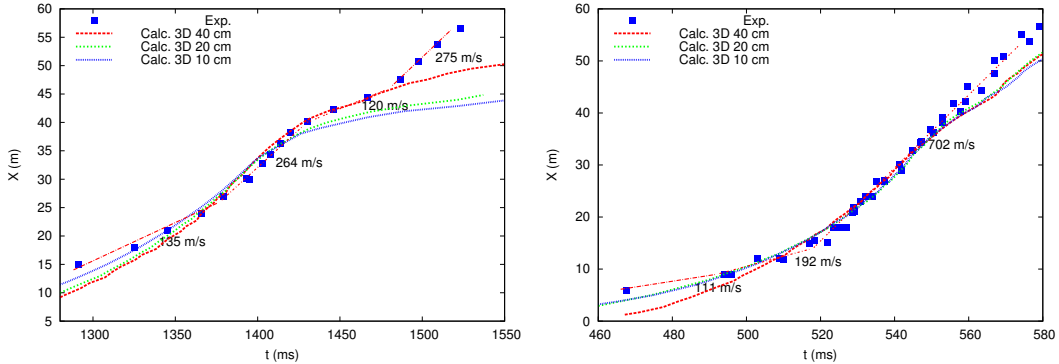


FIG. 6: Grid effect on STH9 and STM7 tests

In the STH9 test (Figure 6), the flame is accelerated in the first channel and consequently slows down in the canyon. These phases are better resolved if the mesh size is below 20 cm. The final phase of flame acceleration in the second channel is not well captured by the model due to the compression waves. In our simulations the volume is closed, while in the experiment, the dead end of the second channel was sealed by wooden and steel plates, which were destroyed when a pressure increased. In the STM7 test (Figure 6), the flame acceleration processes was also well predicted (especially in the range from 10 to 40 m), and no large difference was observed in the results between the mesh size of 20 and 10 cm. The overall effect is due to a better definition of the flame surface compared to the coarse grid of 40 cm. Similarly, the ratio of the r.m.s. velocity  $u'$  to the laminar flame speed  $S_L^0$  can be said to be almost converged as it is shown in Figure 7 at a specific location in the first channel ( $X=22.9$  m).

Consequently, the pressure curves in the STM7 scenario were correctly reproduced in the cases of intermediate and fine grids as it shown in Figure 8 at various locations (experimental pressure signals were filtered by a 100Hz low pass filter). It was, thus, decided to keep a grid size of 20 cm for the following computations (besides for the STH9 test, which is shown next).



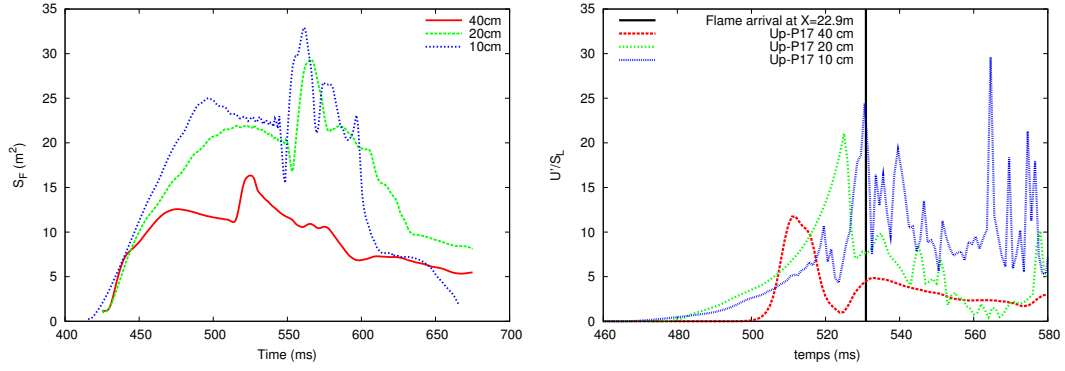


FIG. 7: Grid effect on STM7 test - Flame surface and  $u'/S_L^0$

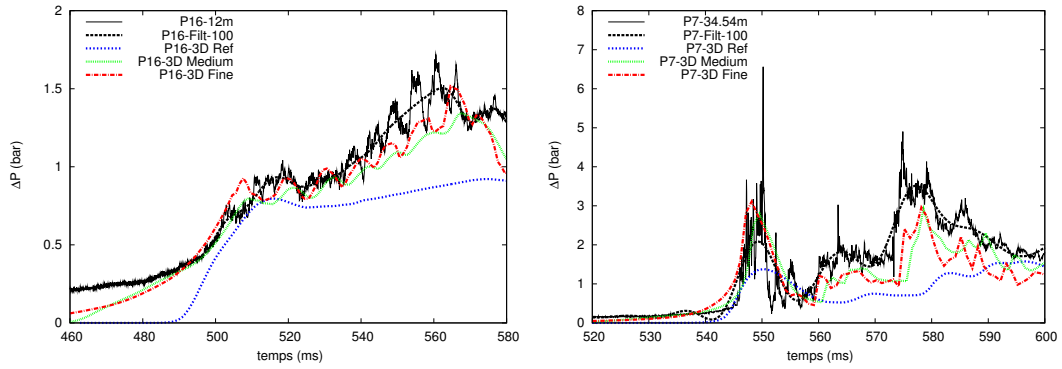


FIG. 8: Grid effect on STM7 test - Overpressures at  $X = 12$  m and  $X = 34.54$  m

The slow flame regime represented a difficulty for the present model. Figure 9 shows that there are almost no grid effect on the overpressure traces for the STH9 case. Although, the computed pressure curves follow a general pressure rise trend, the peaks exist neither in the channel nor in the canyon. This problem can be explained by the appearance of the Kelvin-Helmholtz instability and the subsequent coherent structures behind an obstacle. Changes in the flow structure behind the obstacle or in the canyon lead to changes in dimensions of the integral scales and in the combustion rate, which, in turn, is related to pressure peaks.

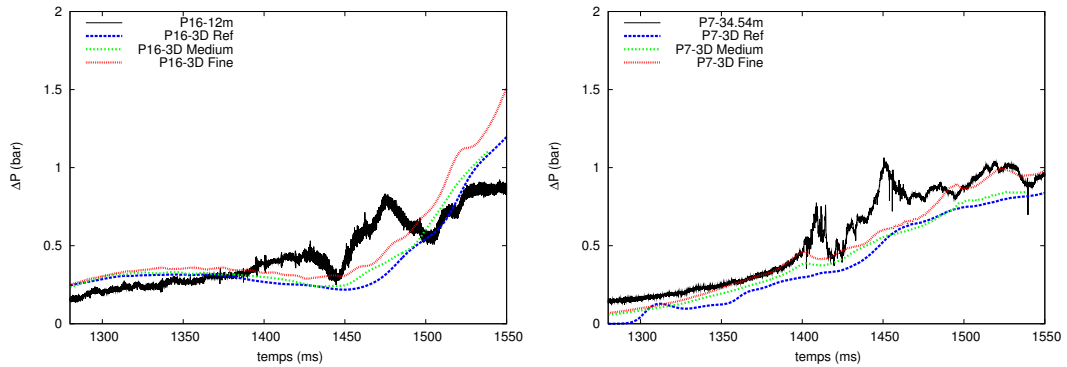


FIG. 9: Grid effect on STH9 test - Overpressures at  $X = 12$  m and  $X = 34.54$  m

As it was described in Section 3.2, the constant integral scale model was improved by introducing the notion of vorticity thickness, in order to characterize growth and development of the separated shear layers. Figure 10 shows the overpressure traces for the STH9 scenario with a corrected model (titled as "NEW" in the figure). It can be seen that pressure peaks are now successfully resolved both in space and time. It should be noted, however, that the new model provides a slightly greater flame acceleration, which is seen in the overpredicted pressure magnitude at later stages, i.e. in the second channel. Figure 11 shows that growth of the flame surface area is quite different for the model with a constant and the one with a variable integral scale, being almost twice as greater for the latter. In addition, it can be seen in Figure 12 that the integral scale in the shear layer zone increases from 0.2 m up to 1 m, which provides necessary local changes to the flame speed and results in a good prediction of pressure peaks.

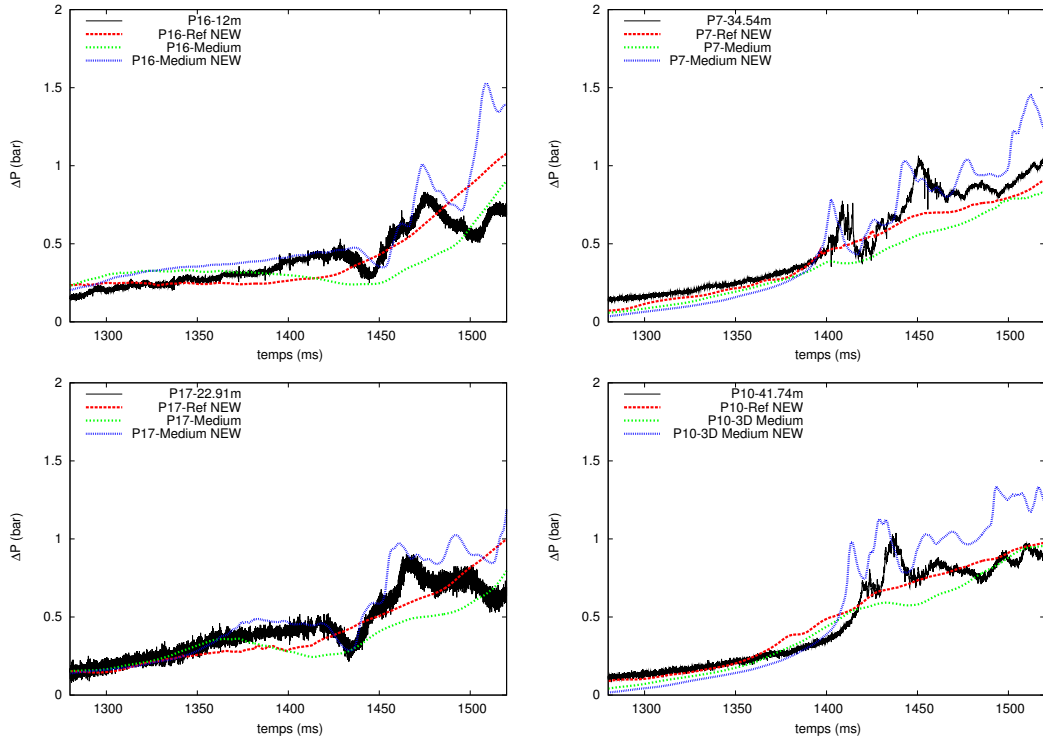


FIG. 10: Model effect on STH9 test - Overpressures at  $X = 12$  m,  $X = 22.9$  m,  $X = 34.54$  m and  $X = 41.74$  m

The steam content generally decreases the reactivity of the combustible gas mixture (diluent effect). Therefore, the STM2 and STM3 test cases with a hydrogen content in dry conditions similar to the STM7 scenario and significantly smaller steam concentrations are shown in Figure 13 to demonstrate the model performance. In the STM2 case both models capture rather well first two stages of the flame development in the first channel: acceleration to the velocities of 157 and 473 m/s until 10 and 20 m, respectively. However, in the last section of the first channel the variable integral model shows better prediction of acceleration phase towards a choked flame. The deceleration stage, which has occurred in the canyon was not captured by both models. Similar results can be observed for the STM3 case. In this scenario the acceleration process was more severe and a transition to detonation was detected in the end of the first channel, but did not last sufficiently long. Although, this behavior

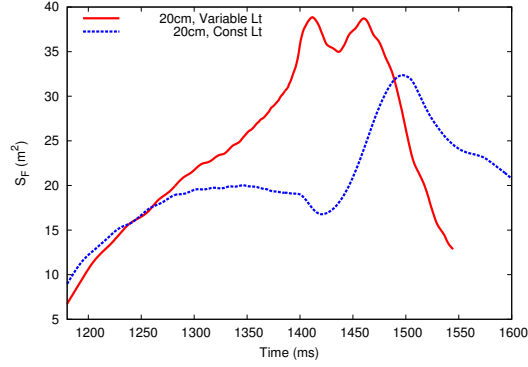


FIG. 11: Model effect on STH9 test - Flame surface

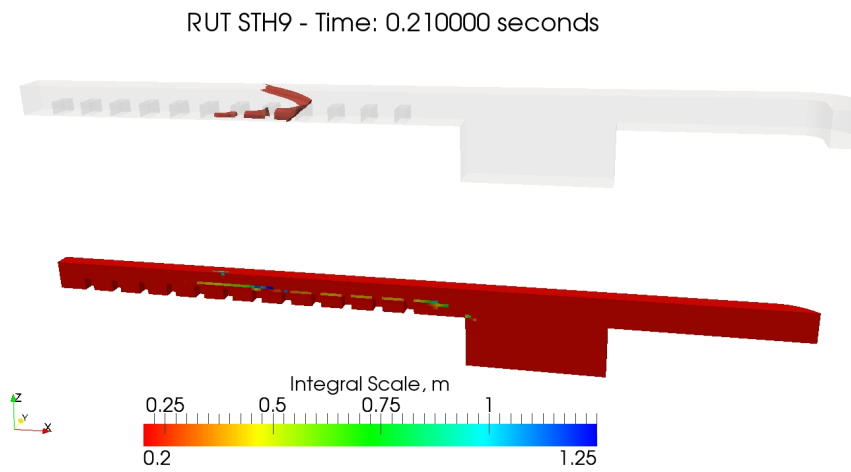


FIG. 12: Model effect on STH9 test - Integral length scale

is well predicted by the models, no deceleration phase in the canyon seems to be observed. However, the pressure traces shown in Figure 14 for the STM3 scenario are rather well captured at various locations (no DDT is registered in the canyon), being over-estimated by the constant integral length scale model. No experimental pressure data is currently available for the STM2 test.

Finally, we show three scenarios from the test matrix performed in dry conditions. The T13 and T23 tests can be compared to see the effect of an increase blockage ratio ( $BR = 0.6$  in the T13 test), while the T23 and T22 cases reveal differences due to an elevated hydrogen content at a given  $BR = 0.3$ . In fact, as it is shown in Figure 15, both models accurately reproduce the flame acceleration in all cases for a limited experimental data set (i.e. only first channel is covered). It can be thought that in the T13 and T23 tests the flame velocity should be increased in the canyon to reach the fast flame regime reported in the experiments. This behavior is correctly resolved by the models. Similarly, in the T22 test case a transition to detonation at the end of the first channel was predicted in computations and observed experimentally.

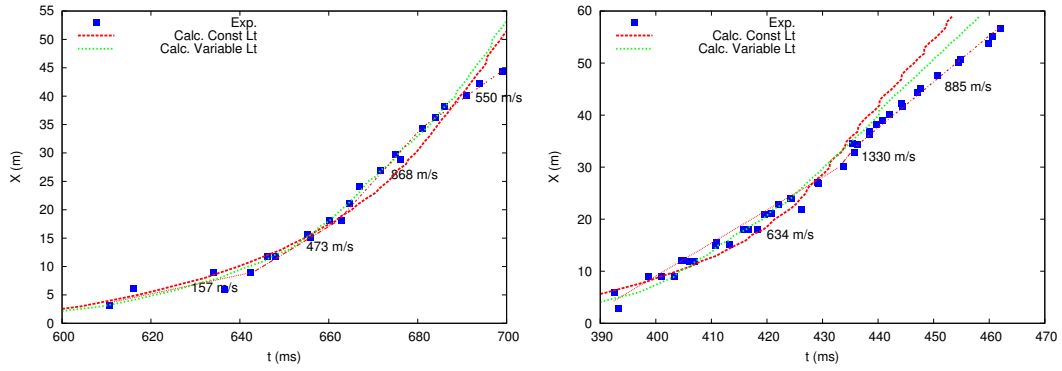


FIG. 13: Effect of steam content at hydrogen concentration close to STM7 scenario: STM2 and STM3 tests

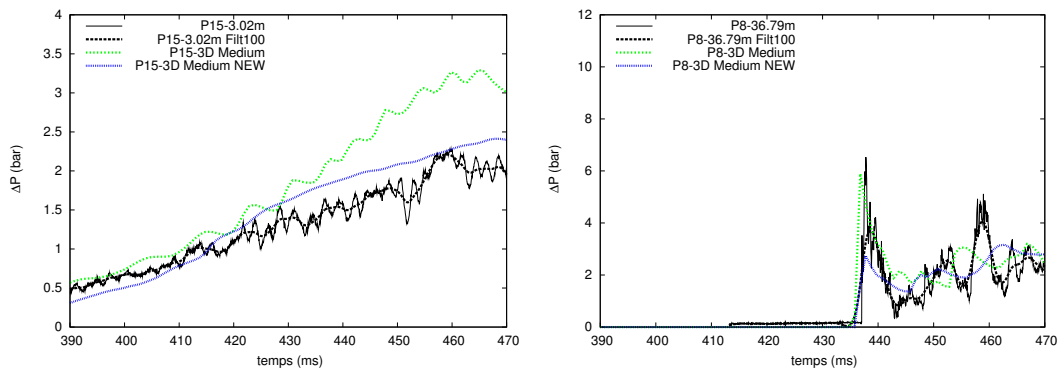


FIG. 14: Effect of steam content in STM3 test - Overpressures AT  $X = 3.02$  m and  $X = 36.79$  m

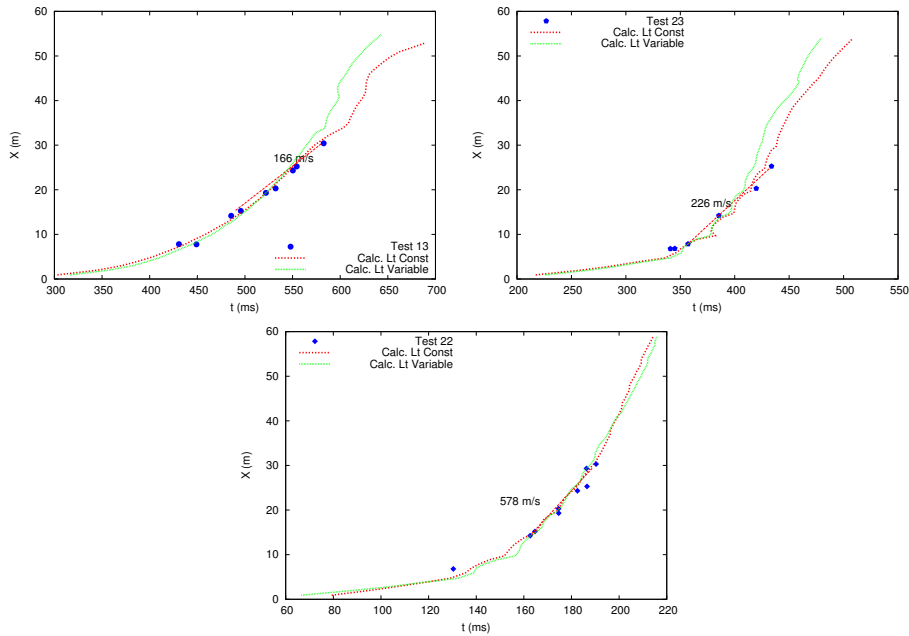


FIG. 15: Effect of blockage ratio: T13 and T23 test, and of hydrogen content: T22 and T23 tests

## 4.2 HDR and FMGlobal facilities

Due to absence of inner obstacles in the geometries considered hereafter, the  $C_u$  was selected to be 0.2 for the constant integral scale model based on the numerical experiments. The second geometry we address is the HDR configuration. Grid sizes of 0.384 and 0.186 m are selected according to the analysis given in the previous section. In addition, to the chambers R1-904, R1-905 and R1-801 with a total volume of 530 m<sup>3</sup>, the dome of 5000 m<sup>3</sup> was also meshed.

Figure 16 shows that the computed pressure traces are only slightly over-estimated by the model (only constant  $L_t$  model was employed). Both grids provide roughly similar results. However, the one with a finer mesh size predicts a more reasonable pressure slope when compared the pressure curve. No attempt to reduce the mesh size was pursued due to the restrictive volume and duration of the experiment.

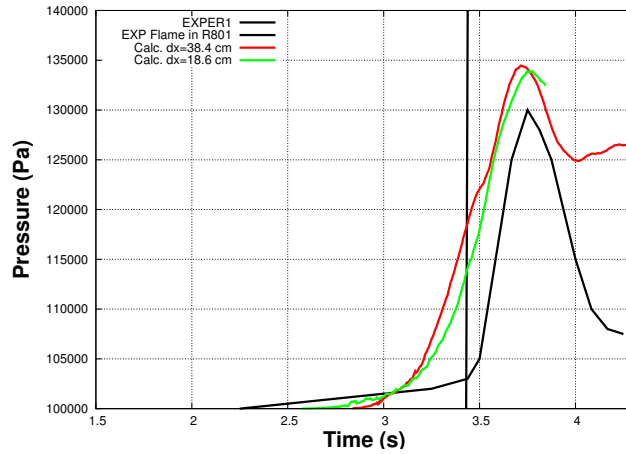


FIG. 16: Pressure history in HDR E12-3-2 test

For the FMGlobal facility only the back-wall ignition case is described herein. The mesh size was chosen to be 0.2 m in the region inside a test chamber, and was progressively increased to 0.6 m towards the boundaries of an external volume, which was set to be as large as 7200 m<sup>3</sup>.

The results of the simulations are shown in Figure 17 together with experimental data for both vent sizes. The pressure increase and the peaks generated by the external explosion are very well captured by the models in the back-wall ignition tests. The greater flame acceleration rate of the variable integral scale model ( $\Theta_{WRIN} = 1$  is employed only in this scenario among those shown herein) is explained by the elevated values of integral length scale in the shear layer region at the time instant when flame front is exiting the vent. No any significant secondary peaks were captured by both models in the back-wall ignition tests.

## 5.0 CONCLUSIONS

A new model to deal with hydrogen combustion in large scale industrial settings has been proposed and extensively validated, demonstrating rather promising results. This model involves only one parameter,  $C_u$ , to be adjusted against experimental data sets. It was

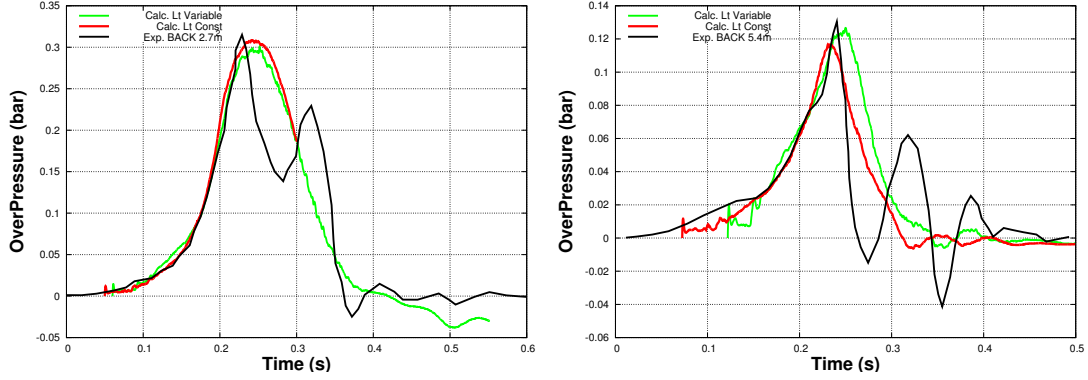


FIG. 17: Pressure history in FMGlobal hydrogen-air mixture back-wall ignition test with a  $2.7 \text{ m}^2$  vent (left) and a  $5.4 \text{ m}^2$  vent (right)

found that  $C_u$  is close to unity in geometries with a series of obstacles (e.g. RUT, DRIVER, ENACCEF, BATELLE), and reduces up to one order of magnitude in vented enclosures with one or several interconnected chambers (HDR, FMGlobal).

The model was improved by introducing the notion of vorticity thickness as an estimate for the integral length scale in the separated shear layer. Following a relative success of this correction it has been generalized for cases when a flame trajectory and a direction of the maximum velocity gradient are not known a priori. This improvement permits to employ the corrected version of the model to study a flame acceleration process under severe accidental scenario in a reactor building. Moreover, the generalized variable integral scale model was seen to be able to reproduce the flame front position without the flame wrinkling factor by a significant increase of the flame surface area (in  $3D$ ). Another avenue for the model improvement, which is also being pursued is flame-acoustic/flame-shock interactions.

## ACKNOWLEDGMENTS

This work has been performed with a support of the CEA GENII/III program. The authors would like to thank V. Fauchet and P. Galon from the Europlexus development team and P. Verpeaux, T. Charras and A. Millard for maintenance of the CAST3M code.

## REFERENCES

---

- [1] Abdel-Gayed, R. G., Bradley, D., and Lawes, M. (1987). Turbulent burning velocities: a general correlation in terms of straining rates. *Proceeding of the Royal Society of London*, A414:389–413.
- [2] Addabbo, R., Bechtold, J. K., and Matalon, M. (2002). Wrinkling of spherically expanding flames. *Proceedings of the Combustion Institute*, 29:1527–1535.
- [3] Bauwens, C. R., Chaffee, J., and Dorofeev, S. (2010). Vented explosion overpressures from combustion of hydrogen and hydrocarbon mixtures. *International Journal of Hydrogen Energy*, 36(3):2329–2336.
- [4] Beccantini, A., Studer, E. (2009). The reactive Riemann problem for thermally perfect gases at all combustion regimes. *International Journal for Numerical Methods in Fluids*, 76:662–696.
- [5] Bielert, U., Breitung, W., Kotchourko, A., Royle, P., Scholtyssek, W., Vesper, A., Beccantini, A., Dabbene, F., Paillère, H., Studer, E., Huld, T., Wilkening, H., Edlinger, B., Poruba, C., and Mohaved, M. (2012). Multi-dimensional simulation of hydrogen distribution and turbulent combustion in severe accidents. *Nuclear Engineering and Design*, 209(1-3):165–172.
- [6] Bradley, D., Law, A. C. K., and Lawes, M. (1992). Flame stretch rate as a determinant of turbulent burning velocity. *Phil. Trans. Roy. Soc. London*, A338:359–387.
- [7] Brown, G., and Roshko, A. (1974). On density effects and large structure in turbulent mixing layers. *Journal of Fluid Mechanics*, 64(4):776–816.
- [8] CAST3M(2012). [www-cast3m.cea.fr](http://www-cast3m.cea.fr).
- [9] Cron, T., Hansjosten, E., Slide, A., and Wolf, L. (1993). Investigation on hydrogen deflagration in a reactor containment. *Technical report, HDR Sicherheit Program*, No 118-93. Kernforschungszentrum Karlsruhe GmbH.
- [10] Dorofeev, S. B., Kuznetsov, M. S., Alekseev, V. I., Efimenko, A. A., and Breitung, W. (2001). Evaluation of limits for effective flame acceleration in hydrogen mixtures. *Journal of Loss Prevention in the Process Industries*, 14:583–589.
- [11] Dorofeev, S. B., Sidorov, V. P., Dvoynishnikov, A. E., and Breitung, W. (1996). Deflagration to detonation transition in large confined volume of lean hydrogen-air mixtures. *Combustion and flame*, 104:95–110.
- [12] Efimenko, A. A. and Dorofeev, S. B. (2001). CREBCOM code system for description of gaseous combustion. *Journal for Numerical Methods in Fluids*, 76:662–696.
- [13] EUROPLEXUS(2012). [europlexus.jrc.ec.europa.eu](http://europlexus.jrc.ec.europa.eu)
- [14] Gostintsev, Y. A., Istratov, A. G., and Shulenin, Y. V. (1987). Self similar propagation of a free turbulent flame in mixed gas mixtures. *Combustion Explosions and Shock Waves*, 24:563–569.
- [15] ISP49(2012). ISP-49 on hydrogen combustion. Technical report, NEA/CSNI/R(2011)9.
- [16] BMC and DN400 Hydrogen Deflagration Tests. Proposal for a test matrix with a link to MUSCET and HDR Tests. *Third Meeting of the Group of Experts on the Development of a Phenomena-based Validation Matrix for Ex-vessel Models and Codes*, January 15-16, GRS, Garching, Germany, 2004.
- [17] Kudriakov, S., Dabbene, F., Studer, E., Beccantini, A., Magnaud, J. P., Paillère, H., Bentaib, A., Bleyer, A., Malet, J., Procheron, E., and Caroli, C. (2008). The TONUS-CFD code for hydrogen risk analysis, numerical schemes and validation matrix. *Nuclear Engineering and Design*, 238(3):551–565.
- [18] Le Métayer, O., Massoni, J., and Saurel, R. (2005). Modelling evaporation fronts with reactive Riemann solvers. *Journal of Computational Physics*.
- [19] Pailhories, P. (2004). Recueil des résultats des essais des combustion hydrogène sur les installations à petite échelle DRIVER et TORPEDO (1999-2001), *Fiche Technique SAGR*, 04-050.
- [20] Malet, F. (2004). *Etude expérimentale et numérique de la propagation de flammes prémélangées turbulentes dans une atmosphère pauvre en hydrogène et humide*. PhD thesis, Université d’Orléans.
- [21] Tennekes, H. and Lumley, J. (1972). *A First Course in Turbulence*. MIT Press.